THESIS FOR THE DEGREE OF LICENTIATE OF ENGINEERING

Experimental Evaluation of a Microwave Imaging System for Muscle Rupture Detection

Laura Guerrero Orozco

Department of Electrical Engineering
Chalmers University of Technology
Gothenburg, Sweden, 2023

Experimental Evaluation of a Microwave Imaging System for Muscle Rupture Detection

Laura Guerrero Orozco

Technical Report No.
ISSN
This thesis has been prepared using LaTeX.

Department of Electrical Engineering
Chalmers University of Technology
SE-412 96 Gothenburg, Sweden
Phone: +46 (0)31 772 1000
www.chalmers.se

Printed by Chalmers Reproservice
Gothenburg, Sweden, February2023

Abstract

Injuries to the hamstring muscles are one of the most common injuries in sports such as football, sprinting, and running. Imaging plays a key role in diagnosing and managing athletes with muscle injuries, and particularly magnetic resonance imaging is usually required to diagnose muscle ruptures. Unfortunately, this imaging modality is both costly and availability is limited. The aim of this work is to explore the possibility of using a microwave imaging system to aid in the diagnosis of a muscle rupture and eventually supplement or perhaps even replace current imaging modalities. A microwave based imaging system could help improve availability and bring the cost down leading to improved and more accurate diagnostics.

The microwave imaging system consist of several antennas placed on a semi circular array. The antennas consists of monopole antennas and a lossy (conductive) gel. The lossy gel serves the purpose of reducing the effects of signals taking undesired paths outside the body under test and improves the image quality. In this work, different gels were manufactured and evaluated in imaging experiments. The results show that the lossy gels can effectively reduce the undesired signals, resulting in significantly more stable and repeatable image reconstructions. The results were consistent in several different imaging experiments with targets of different size and location.

Furthermore, a software defined radio (SDR) board was explored and benchmarked against a high-performance Vector Network Analyzer (VNA) with the purpose to assess whether it could be used as a low-cost and compact alternative for the measurements. The measurements showed good repeatability and accuracy for a transmission loss up to 70 dB, with the option to adapt the system gain to handle even higher transmission losses in specific channels.

Keywords: Microwave imaging, medical diagnosis, antenna system, muscle rupture, SDR.

List of Publications

This thesis is based on the following publications:

[A] **Laura Guerrero Orozco**, Lars Peterson, Andreas Fhager, "Microwave Antenna System for Muscle Rupture Imaging with a Lossy Gel to Reduce Multipath Interference". Published in Sensors 2022, 22, 4121.

[B] **Laura Guerrero Orozco**, Lars Peterson, Andreas Fhager, "Muscle Rupture Microwave Imaging with a Lossy Gel to Reduce Multipath Interference". Acepted for publication at 17th European Conference on Antenna and Propagation.

[C] Xuezhi Zeng, **Laura Guerrero Orozco**, "Measurement quality of a software defined radio system for medical diagnostics". Published in the Journal of Engineering-JOE, Volume 2022, Issue 12 December 2022 pages 1162-1172.

Other publications by the author, not included in this thesis, are:

[D] **Laura Guerrero Orozco**, Andreas Fhager, "Study of a system for stable microwave image reconstruction applied to muscle rupture detection". *ESHO2022*, 34th Annual Meeting European Society for Hyperthermic Oncology, 14–17 September 2022, Gothenburg.

[E] Phase calibration of a software defined radio system for medical applications, "Xuezhi Zeng, and **Laura Guerrero Orozco**, Andreas Fhager". *2019 IEEE Asia-Pacific Microwave Conference, APMC 2019* Singapore, Singapore, 2019-12-10 - 2019-12-13.

Acknowledgments

I am deeply grateful to my supervisor Andreas Fhager. Thank you for your invaluable patience and feedback. You have been solid as a rock an it would have been impossible to accomplish this work without your guidance. I would like to express my sincere gratitude to my co-supervisor, Xuezhi Zeng, thank you for guiding me since I was a master student, your encouragement made it possible for me to be here.

I would like to extend my sincere thanks to my colleagues in the Biomedical Electromagnetics group: Hana Dobsicek Trefna, Mikael Persson, August Ekman and Alejandra, and former colleagues Samar, Morteza, Jan and Karan. A special thanks to my colleagues turned friends Moein, Mattia, Gabriel, Yara, and Rita. Thank you for your support and for all the times we have laughed together in the kitchen.

I would like to thank my friends Dmitrii aka, Chouaib, Asta & Mauricio (Masta), Lewis, Roman and Guzal.

Last but not least, I would like to thank my parents and brother back home for always supporting me.

Acronyms

OUT:	Object Under Test
SDR:	software defined radio
VNA:	Vector Network Analyzer
DMAS:	Delay Multiply and Sum
UWB:	Ultra wide band
PLL:	Phase locked loop
SNR:	Signal to Noise Ratio

Contents

Part I

Overview

CHAPTER 1

Background

Muscle strains and complete ruptures are common for athletes across many disciplines, representing 30% or more injuries seen by clinicians in sports medicine practice [1]. This normally happens in sports such as sprinting, running, soccer, and gymnastics [2], [3], and can happen anywhere in the body but are most common in the muscles composing the hamstring [4]. Along with a physical examination, imaging plays a key role in the diagnosis and management of athletes with muscle injuries. The gold standard diagnosing method chosen by radiologists and clinicians is magnetic resonance imaging (MRI) [5], Unfortunately, MRI is a very limited and expensive resource. Especially for non-elite sports teams, this is not a viable option since there may be many athletes suspected of having muscle injuries every training that one ideally would like to examine. Another imaging modality that is becoming popular is sonography since they are portable and low cost[6]. Unfortunately, sonography still needs a specialized operator and the result of the examination is extremely operator dependent [5]. The operator needs to have specific knowledge of compartmental muscle anatomy as well as experience in assessing normal and abnormal muscle tissue during different healing phases[7]. Ultimately these imaging methods are only used in cases where there are acute injuries due to the costs and inconvenience accompanying these imaging modalities. It is not necessary to be a professional or semi-professional athlete to get these types of injuries. More people are participating in recreational sports, and these injuries are also occurring in people among the general population. Regrettably, the prevalence of hamstring tears in recreational sports and non-sporting situations is not well defined [8], [9] but if imaging is already to some extent limited for professional athletes, when the non-professionals or recreational athletes get injured it might not be valued as enough to afford the costs associated with imaging, even in cases where it would be favorable for the diagnose and, therefore, treatment of the patient. This is where microwave imaging can be a game changer. Microwave imaging has seen an increase in the last couple of years due to advances made by cellular technology, we are developing a technology that can be cheap to manufacture and portable. Our vision is that a device developed with this new technology could be present in sports clubs or game locations and used by coaches or medical staff present to help diagnose and triage the presence of a muscle rupture and administer proper care for the athlete.

1.1 Anatomy and injuries of hamstring area

The thigh is composed of three compartments, that is to say, three limited spaces with big muscle groups that are separated by connective tissue membranes (called fascia)[10]. A cut through a cross-section of the thigh (Figure 1.1) shows the adductor (medial compartment), the quadriceps in the anterior compartment, and the hamstring in the posterior compartment. Figure 1.2 shows the three long muscles in the posterior compartment of the thigh that compose what is known as the hamstring: the biceps femoris caput longum, biceps femoris caput breve, semimembranosus and semitendinosus muscles. The hamstring muscles flex the leg at the knee joint and extend the thigh at the hip joint, they also function as rotators. Muscle strains can be wear and tear or impact injuries. These injuries in the thigh are common in sports that involve explosive moments like football and running as well as in sports where jumping is involved. All muscles in the thigh can be affected but the most affected muscles are the ones composing the hamstring area [11]. Hamstring injuries often happen in the biceps femoris and semimembranosus 66% of the time. Multiple injuries involve the biceps femoris and the semitendi-

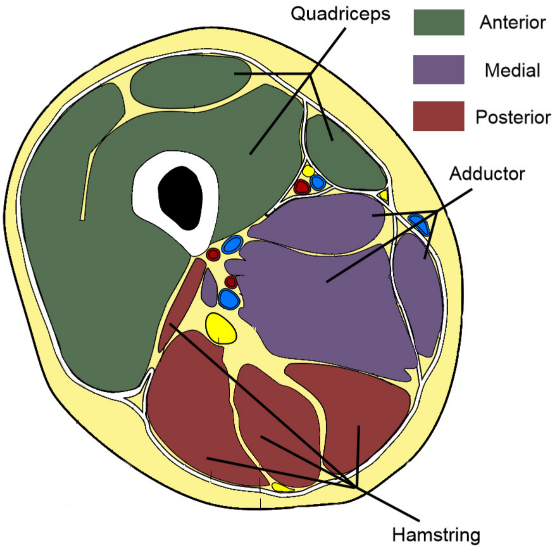

Figure 1.1: Medial cross-section of thigh showing three compartments.

nosus around 33% of the time. For elite athletes in track and field, the biceps femoris muscle was the most commonly affected muscle being involved in 75% of injuries and the connection between the muscle and tendon (musculotendinous junction) was involved in 93% of lesions [12]. In English professional football (premier and football league) hamstring strains accounted for 12% of the total injuries seen over two seasons, this being the most prevalent injury, with 53% of the injuries involving the biceps femoris muscle [13]. Each English club sustained an average of five hamstring injuries per season, a comparable result with Australian football where clubs averaged 6 hamstring strains per season [14].

One explanation for the high incidence of injuries in the area is that this muscle group functions between two joints, therefore it needs to stretch at more than one point [15]. Additionally, the hamstring muscles have a muscle-tendon junction for almost the entire length of the muscles creating weak spots in the muscle and making it possible to have a muscle strain at any point in the muscle [10], [11].

These types of injuries have a high percentage of relapse, between 12-43%

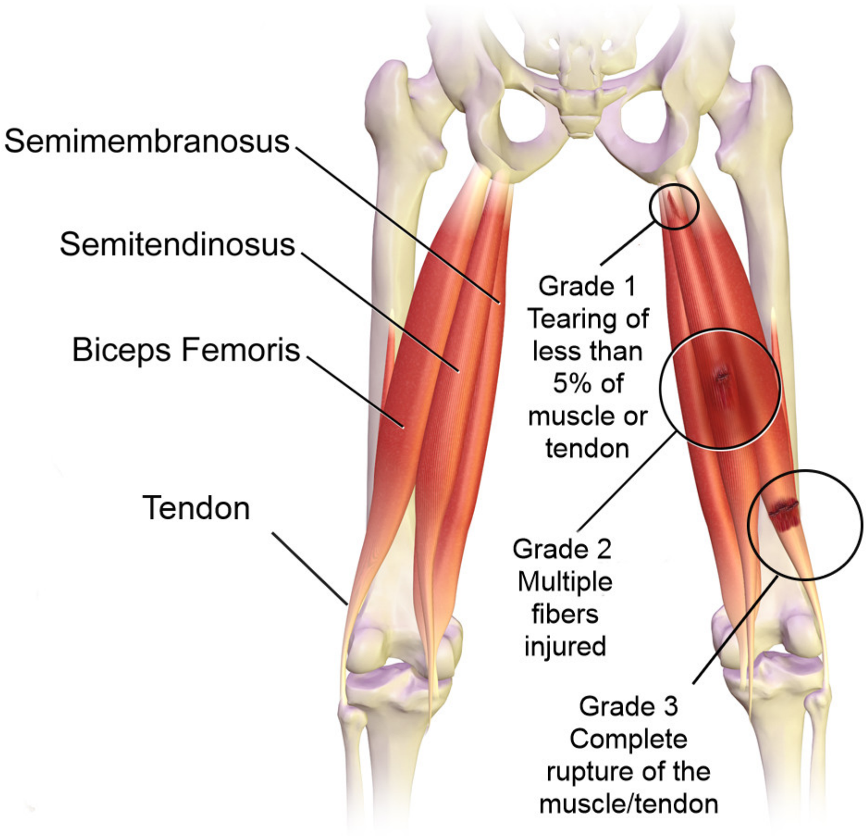

Figure 1.2: Anatomy of the hamstring muscles and muscle ruptures.

[11], [13] with the re-injury rate being the biggest frustration when dealing with hamstring injuries [13], [16]. These injuries represent a high percentage of downtime for athletes[11], [13], [14]. Symptoms often persist for a long time and healing time can reach up to 12 months in severe cases [16]. In rugby, on average, injuries resulted in 17 days of lost time, with recurrent injuries presenting a longer lost time compared to new injuries [17] and recovery time ranging from 2 to 6 weeks in track and field athletes[12].

Clinical evaluation

The symptoms of a rupture in the hamstring muscles is intense pain in the back of the thigh that arises after a sudden movement. It could typically feel like being stabbed by a knife [11] and the pain can be even more severe when the injured muscle is moved. It has been shown that a secondary effect of the injury is inflammation and edema [18]. After the symptoms start a clinical evaluation should be done within 1 or 2 days [11].

The evaluation can include the following tests [12]: inspection for bruising, ability to walk without pain, palpation of the posterior thigh with the athletes in the prone position (face down) to feel the presence of tenderness in the area, pain in movements like hip flexion, measurement of active range of motion (AROM) of the knee in the injured and uninjured side. In more extensive ruptures a gap can sometimes be felt in the musculature, but this is not typical for smaller ruptures.

After the clinical evaluation, the grade of the injury will be assessed as well as the treatment options. Muscle strains are divided into three grades depending on the severity of the injury (Figure 1.2). Grade I represent a minimal injury representing less than 5% of the muscle injured with only a few muscle fibers torn. Grade II is a partial tear that involves between 5-50% of the muscle and can be treated with physiotherapy starting a couple of days after the injury. In some cases, a hematoma can make it necessary to have a fasciotomy to relieve pressure in the compartments of the thigh. Grade III represents a complete rupture and should be treated with surgery [11], [19].

Most hamstring injuries that are diagnosed are managed with conservative treatment, meaning that imaging is not always performed [15]. Whether imaging is necessary for the assessment of posterior thigh injuries in athletes is a debated topic [12]. Using a conservative diagnosis, by only performing a clinical evaluation as the one described before, is not a bulletproof approach since there are other structures other than the hamstring muscles themselves that can be responsible for posterior thigh pain, and a correct diagnosis is essential to find adequate treatment. For example, minor-grade hamstring injuries have considerable overlap in clinical features with injuries involving referred pain (when the pain felt in one part of the body is actually caused by pain or injury in another part of the body)[20].

Current imaging methods

When deciding to use imaging techniques, the clinician must take into consideration the cost factor. Imaging techniques, such as MRI show detailed information about the injury where even minimum injuries involving less than 5% of the muscle can be identified [11]. However, simpler clinical techniques would be preferred from a cost and availability point of view [21]. On the other hand, ultrasound is a cheaper and more accessible modality but even taking this into account some clinicians do not use ultrasound scans for grade I and grade II injuries in an attempt to keep the diagnosis at a lower cost [12].

Imaging should be done in the same time window as the clinical evaluation (1-2 days), so there is a time constraint. Imaging is more likely to be performed early in elite athletes, in cases where there is severe pain [15]. Minor injuries, like minor strains (injuries that may impair performance but do not limit participation), are usually not deemed important enough to afford the cost of imaging and thus are also less likely to be recorded in literature [22]. Minor injuries, grade I and II, should not be completely disregarded as they may lead to more serious re-injuries, and here is where microwave imaging would be the most useful.

1.2 Introduction to microwave imaging

Microwave based imaging and diagnostics have gained increasing popularity in recent years and could be a competing technique or supplement for the current imaging modalities used for muscle rupture detection. Microwave imaging has been used for decades in long-range applications like marine radars and weather radars but in recent years short-range applications have gained attraction, an example of this is surveillance for concealed weapons in airports [23]–[25].

There are two reasons why this technology is interesting for biomedical applications. The first is the operating frequency range. The technology exploits electromagnetic radiation that goes from several hundred MHz to several hundred GHz with wavelengths (λ) ranging from 1 m to 1mm. These wavelengths are similar to dimensions inside the body [26], [27]. This allows for enough resolution to create an image presenting a map related to the dielectric properties in a region of the body. The choice of an appropriate frequency range to use in this application is vital, the higher the frequency the shorter the distance the field can penetrate into the body. Therefore, frequencies above 10 GHz might not give much information about the deeper part of the body making them more appropriate for surface applications instead. The second is that there is a contrast in the dielectric properties, permittivity (ϵ_r) and conductivity (σ), that is naturally found in different tissues in the body [28], [29]. When an electromagnetic wave encounters the interface between tissues with different properties the wave will divide, a part of the wave will continue to transmit and a part of the wave will reflect. The proportion of the wave transmitted and reflected will depend on the difference in properties between the tissues in the interface, this will create a change in the magnitude and phase of the electromagnetic wave that can be sensed using an antenna. These factors make microwave diagnosis and imaging of different ailments possible due to changes and abnormalities in the dielectric properties.

Microwave imaging has been studied in many applications over the years. The medical diagnosis applications are for example: breast imaging [30]–[32], brain imaging [33], [34], kidney imaging [35], cardiac imaging [36], bone density measurements [37] and compartment syndrome [38].

Approaches to microwave imaging

There are two main approaches to microwave imaging. One approach called microwave tomography forms images of dielectric properties from measurements of electromagnetic waves that have propagated through the tissue [39]. Microwave tomography belongs to a group of imaging techniques based on solving inverse scattering problems. Reconstruction algorithms are used to create maps of the dielectric property distribution of the body part [40]. Many tomographic algorithms optimize the solution by comparing the measurements with the results of numerical simulations that are iteratively refined to better fit the measured data.

A second group is radar-based approaches which use time-of-flight measurements to form images that indicate the location of strongly scattering objects [41]. Radar-based imaging, also called Confocal Microwave Imaging, creates an intensity map showing the location of a strong scattering object, rather than creating a map of the distribution of dielectric properties. In our application to detect muscle ruptures, the algorithm takes advantage of reflections from within the leg due to the presence of blood [42]. It provides less detailed information about the body but uses simpler imaging algorithms. Radar-based systems have a lot in common with ground penetrating radar systems for object detection as both systems detect an anomaly in a heterogeneous background [27].

Properties of leg tissue in microwave region

The permittivity in the MHz to GHz range is mostly dependent on the water content found in the tissue, for example, the permittivity of low water content tissues like fat and tumors is lower than high water content tissues like muscle and skin (Figure 1.3a). On the other hand, conductivity depends mainly on the presence of ionized atoms due to different dissolved substances, like salts or sugars in the tissue (Figure 1.3b). Additionally, the dielectric properties of tissues exhibit strong dependence on frequency (frequency dispersion) in the RF and microwave bands.

Phantoms and tissue-like media

In order to do measurements it is desired to make phantoms that are designed with similar permittivity and conductivity to the dielectric properties found in the leg. Phantoms can be made using liquids, like glycerin [43], using Triton X-100 [44] gels [45], rubber like liquids, and solid materials [46]–[48]. For the experiments explained in later chapters, muscle and blood phantoms were manufactured using water, salt and sugar to act as a solvent, control the conductivity and control the permittivity respectively. Agar was used to make the phantom mix solid [49]. We decided to use water, salt, and sugar because the manufacturing process is simple, the ingredients are harmless and the mimicking of the dielectric properties of the body is good enough for proof-of-concept experiments. The properties of the phantoms can be found in Paper A.

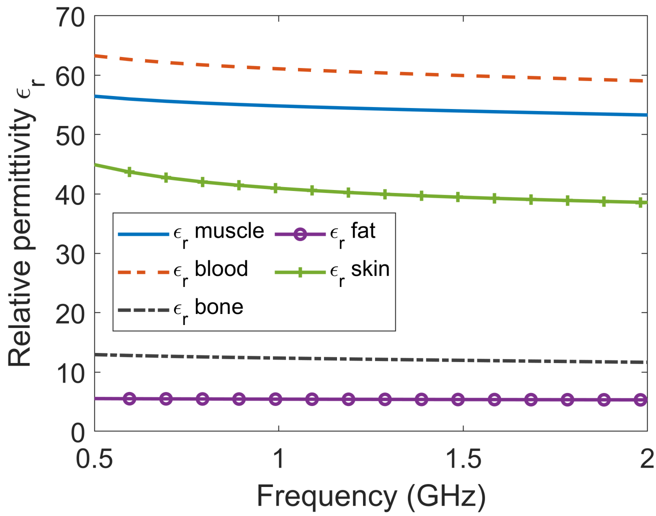

(**a**) Relative permittivity ϵ_r

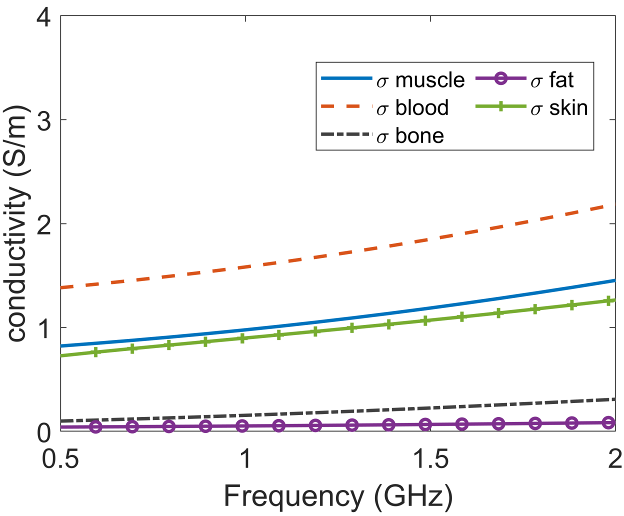

(**b**) Conductivity σ(S/m)

Figure 1.3: Permittivity and conductivity of different tissues in the leg.

1.3 Aim and thesis outline

The aim of this project is to explore the possibility of using microwave imaging for the diagnosis of muscle rupture. The aim is to create a radar-based imaging system that, as a long-term strategy, also permits the use of tomographic algorithms. Although a successful diagnostic method could be based on confocal imaging algorithms, it is not unreasonable to look for a solution that also works with tomographic imaging as the dielectric properties may contain important information that can help diagnose a patient with muscle ruptures. In the spirit of making the running time of tomographic algorithms shorter, the use of simple antennas (e.g., monopoles and dipoles) is desired to avoid complexity in the numerical models needed for the optimization of these algorithms. Therefore, the aim is to create an imaging system using monopole antennas. To accomplish this aim the use of lossy gels is explored to help attenuate multipath signals and increase image quality while using low-profile antennas such as monopoles, as shown in papers A and B. Another aim is to study the measurement quality of the Software Defined Radio (SDR), a system that is used for wireless communications, for medical applications. This is explained thoroughly in paper C.

The thesis contains two parts. Part I has 5 chapters. Chapter 1 provides a background for a better understanding of the problem and states the aim of the thesis. Chapter 2 gives a brief overview of measurement systems as well as antenna arrays, the antenna used in this project is introduced as well as some results obtained using the lossy gel. Chapter 3 the different approaches to microwave imaging are explained with some experimental image reconstructions shown. Chapter 4 presents a summary of the appended papers. Finally, chapter 5 concludes the thesis and discusses possible directions for future work. Part II contains the main contributions of the author in the form of appended papers.

CHAPTER 2

Experimental systems

Microwave imaging systems consist of a measurement system, an antenna array, and a computer that contains the microwave imaging algorithm. In this section, we will briefly introduce and discuss measurement systems and antenna arrays.

2.1 Measurement systems

Microwave imaging systems can be based on single frequency, multiple frequency, or ultrawide band (UWB) data, Where UWB refers to a bandwidth greater than 20% of the center frequency or 500 MHz. In practice, measurements can be carried out using frequency domain systems or time domain systems. There are many examples of each type of system used in research [50]–[54]. Most of the research aiming at proof-of-principle has been conducted using costly and bulky lab equipment like VNAs or oscilloscopes, however more compact and low cost measurement systems are desired to facilitate clinical adaptation. This is the reason why many research groups have started working on the minimization of systems using either compact commercial instruments or custom build systems [34], [55]–[58].

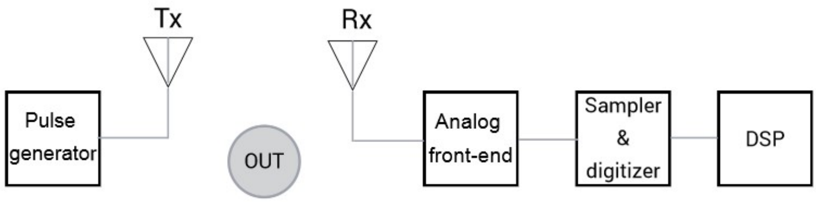

Figure 2.1: System block diagram of a time domain measurement system for microwave imaging.

Time domain systems

The system block diagram of a typical UWB time domain measurement consists of a pulse generator that illuminates the object under test (OUT) and the time domain response signal is acquired by the receiving antenna where it is sampled and digitized for use in the image reconstructions. This is depicted in Figure 2.1. Time domain systems usually use a sampling or high speed real-time oscilloscope as receivers.

These types of systems are attractive for medical applications since they have the inherent advantage of having a fast acquisition of UWB data since some real-time oscilloscopes are capable of acquiring a pulse with single shot measurement. There are many examples of experimental systems working in the time domain [50], [51], [59].

Breast cancer imaging is one application where UWB data has been utilized and there are several examples where solutions have been developed for the miniaturization of systems. In [55] an integrated stepped-frequency continuous-wave (SFCW) UWB radar transceiver was custom designed to work in a breast imaging system. An integrated circuit pulse radio was used in [57] to replace a bulky and expensive pulse generator. Zeng et al. worked towards the development of miniaturized systems for microwave tomography with the long term goal of having a system-on-chip [56], [60].

Frequency domain systems

Another common method to perform microwave measurements is through the frequency domain. An example of such technology is a Vector network analyzer (VNA).

The architecture of VNA is shown in Figure 2.2. The measurement procedure starts with a radio-frequency (RF) generator that produces a single frequency test signal which is used to illuminate the OUT. The response of the object at this frequency is recorded by the receiving antenna. The received signal is first amplified using a low noise amplifier (LNA) and down-converted to an intermediate frequency (IF) through a mixer. The signal is passed through a narrow band IF filter that is used to eliminate interfering signals at other frequencies and this output is sampled and digitized with an analog-to-digital converter (A/D) with high accuracy and the output digital data is processed with a digital signal processing module (DSP). Amplitude and phase are obtained.

The response of the OUT at several different frequencies can be obtained by step-wise changing the frequency of the generated test signal. A time domain pulse can be synthesized with a Fourier transform from the frequency domain scattering data obtained [61], [62].

VNAs are supported with powerful measurement platforms as well as calibration functions that can provide ready to use high accuracy solutions for experimental use, making them really relevant in research [52]–[54], [63], [64]. A disadvantage is that VNAs suffer from long settling times due to the need for narrowband filters or slow synthesizers. Therefore, the measurement speed is quite limited, especially when doing UWB measurements.

In recent years there has been a trend in developing compact VNAs and most major manufacturers offer a variety of alternatives. Compact VNAs have been used to make portable systems to facilitate clinical trials in stroke detection [34], [65], as well as to detect head injuries in experiments using phantoms[58].

Software defined radio

Software Defined Radio (SDR), refers to a wireless communication technology in which the transmitter modulation is generated or defined by a computer [66]. Large parts of the waveform are defined in software, giving the flexibility

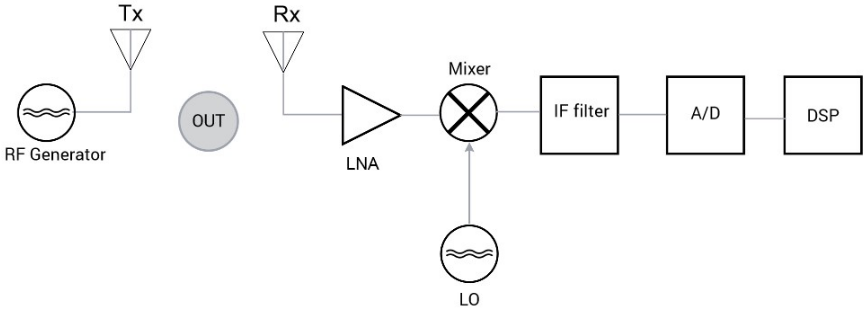

Figure 2.2: System architecture of VNA for microwave imaging.

to change the waveform within certain bounds, also extend the flexibility to multi-band transmission. The demand for flexibility in communication applications has made the SDR a technology that is useful in many areas within wireless systems. It is very interesting in particular for the military sector, an area that has been the driving force in the development of this technology[67]. As mentioned before, for pre-hospital diagnosis a small, cheap, and accurate system is necessary. SDRs are very compact in size and are significantly lower in cost compared to a VNA, therefore it is interesting to explore if such systems could replace VNAs in microwave diagnostic applications.

As a device made for wireless communications the SDR cannot be completely classified as a frequency domain system or a time domain system since it presents qualities found in both types of systems, but due to its flexibility, it has the possibility of being operated in a way that resembles a frequency domain system.

Figure 2.3 shows the principal block diagram of a typical one channel SDR system. A single tone signal is created in the digital domain (DSP), this digital signal is then interpolated through the digital up converter (DUC) and converted to an analog signal by the digital-to-analog converter (D/A). The analog signal will then be further filtered, modulated to a higher frequency, and amplified before being transmitted out by an antenna using the mixer and a variable gain power amplifier (VGPA). A similar process will be followed by the received signal. The received signal will be amplified with the necessary gain (using a variable gain amplifier(VGA)) and then down-converted to an

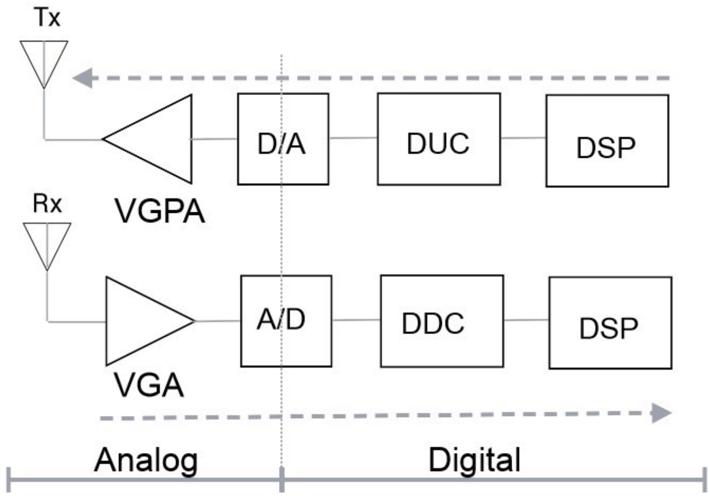

Figure 2.3: Simplified system architecture of SDR.

intermediate frequency in order to facilitate the analog to digital conversion (A/D). The obtained digital data will be further down-sampled by the digital down converter (DDC) before being transferred to a DSP for processing.

Also with an SDR, wide-band measurements can be done with a stepped frequency approach and due to the variable gain in both transmitters and receivers the system can potentially give a high dynamic range. This makes the system appealing for medical applications where the signal varies in strength.

In paper C the measurement quality of an SDR board is explored. The investigated system is a two-channel SDR board USRP 2901 from national instruments [68] which is equivalent to the Ettus Research USRP B210 board.

For imaging applications, accurate measurements of both amplitude and phase are desired. A common problem found in SDRs is the use of two different phase-locked loops (PLLs) to generate the carrier frequencies for the transmitter and the receiver. Both of them use the same reference input clock but the output clock signals are not synchronized so the phases of the generated clocks are random and vary from run to run. As consequence, the measured phase will also be random and cannot be correlated to the object response. A calibration strategy is shown in paper C to make these phase measurements stable.

In [69] Marimuthu et al. have proposed a monostatic SDR based UWB head imaging system where they demonstrated image reconstructions of simple objects and in [70] eventually developed a multistatic imaging system composed of a SDR board and a switching matrix. Meaney et al reported a sixteen channel tomographic system that is composed of nine SDR boards [71].

2.2 Antennas and antenna arrays for imaging

Antennas are used to transmit microwave signals into the OUT and to receive them once they have propagated and scattered through the OUT. To date, numerous different antennas have been proposed for microwave imaging applications in different parts of the body [30], [72]–[77]. These antennas are configured into an array, which for biomedical applications, usually is a circular configuration. However, other configurations are also possible such as half circles, and half spheres [39], [72], [78], [79]

A typical measurement system consists of an antenna array as shown in Figure 2.4 with the OUT in the center of the array. All antennas can be operated as both transmitters and receivers, whereby one antenna at the time usually transmits whereas the other antennas receive. Measurements are repeated until all possible combinations of transmitting and receiving antennas have been used.

Multipath signals

The interesting parts of the signals are those that originate from the transmitter, enter into and scatter within the object, and are picked up by the receivers. As seen in Figure 2.4 the antennas are positioned close to each other, which inevitably will result in other signal paths than through the OUT, for example, reflections from parts of the antenna system and the surrounding environment, direct coupling, and multipath signals between antennas. As these signals also tend to be large in amplitude, and even very small variations from measurement to measurement can introduce unpredictable inconsistencies in the signals. As a result, image reconstruction becomes prone to containing artifacts, which is shown and discussed in papers A and B.

The signals taking alternative routes, like surface waves, reflections and

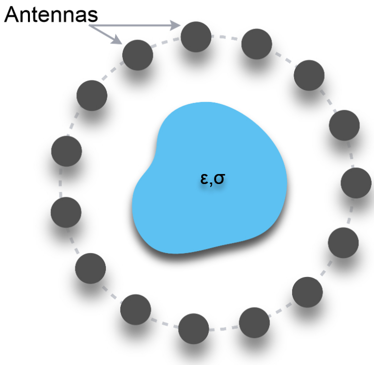

Figure 2.4: Schematic representation of an imaging system.

scattering from the antennas themselves, reflections of supporting structures, cables, the surrounding environment, or the cross-channel leakage in the electronic system [80] are undesired and carry no information from within the OUT. These unwanted signals cannot be filtered out easily since they all originate from the same source as the desired signals, use the same frequency, and only appear as interference. In near-field applications especially in biomedical applications, where the signals are heavily attenuated by tissue the multipath propagation can become problematic and the useful signal can drown in the much stronger but unwanted signal paths. Additionally, the dielectric properties of biological tissue are very different from the dielectric property of air, this leads to a high degree of scattering from the interface between the air and the body part, leading to low signal power entering into the OUT.

In order to decrease the signals going around the object and reflecting from surrounding structures, it is desired to maximize the power penetrating into the body while minimizing the power propagating on the outside of the OUT. For deeper penetration two approaches have been proposed [24]: design antennas with a high directivity that focuses a larger part of the energy into the OUT or use coupling liquids that help couple the energy into the OUT by impedance matching and at the same time attenuate energy outside the OUT.

Directive antennas

In this approach, both off-body and on-body antennas are designed to maximize the energy that is coupled into the OUT and minimize the power radiating in other directions. With a good impedance matched antenna and the main radiation lobe directed towards the body, the multipath effects from waves traveling outside and around antennas are minimized. There are several examples of such antenna designs [30], [72]–[77]. These antennas usually come with the advantages of having broader operating bandwidths, and unidirectional radiating patterns with high gain. They can also be designed to be relatively small in order to have a sufficient number of antennas in the imaging system.

Unfortunately, these antennas also come with the disadvantage of increased complexity, which is a problem in microwave tomographic algorithms as it results in more complex and more computationally demanding simulation models [52], [81]. This means that these antennas are less suited for tomographic algorithms, but more suited for radar-based algorithms.

Coupling liquids

This approach uses coupling liquids to lower the contrast between the media and the biological tissue. The first coupling medium used in experiments was water by Larsen and Jacobi [82], [83]. Since then many different liquids have been explored [84]–[86]. In some systems, saline solutions, or mixtures of glycerine and water have been used to create a lossy coupling bath [52], [87]. By immersing antennas and OUT in a lossy coupling bath unwanted multipath signals can be attenuated [86]–[88]. At the same time, the coupling liquids provide impedance matching between the antennas and objects, thus maximizing the energy coupled into the OUT. The lossy liquid has the additional advantage of broadening the operating bandwidth of the antennas due to resistive loading. This permits the use of low profile antennas, such as monopoles or dipoles, in a wide frequency band [89] which are less complex to model and therefore more suitable for tomographic imaging.

2.3 Antennas for muscle rupture detection

As explained before even though our hypothesis is that muscle rupture diagnostics could be attempted using radar-based imaging, quantitative imaging would give more information about dielectric properties that may be important for the diagnosis of the patient. This is the reason why a design using simple monopole antennas is suggested in this work.

Simpler monopole antennas seem to be effective in applications that aim for quantitative image reconstructions [52], [90], [91] and a fast reconstruction algorithm based on the 2D discrete dipole approximation was developed by Hosseinzadegan et al.[52]. This algorithm takes advantage of the low profile monopole antennas, which can be modeled efficiently as a line source. A lossy coupling bath, made of water glycerine mixtures, ensures the reduction of unwanted multipath signals, for example, scattering from the wall of the imaging tank and the antenna elements themselves.

A liquid coupling bath is not very practical for the muscle rupture application as it means that the leg needs to be immersed in the bath for the measurements. Our goal was instead to investigate the design principles of an antenna system that is adapted for muscle rupture imaging without having to immerse the entire leg, in a tank filled with liquid.

In paper A, we present an antenna design that makes use of a semisolid gel consisting of a mix of saline water and agar to recreate the effects of antennas in a lossy bath [86], [88]. The goal was not to completely eliminate multipath signals but to attenuate them sufficiently to avoid corruption in the measured signals and image reconstruction.

The antennas we use for the muscle rupture detection application are shown in Figure 2.5. These are monopole antennas manufactured by peeling off the outer conductor from a semi-rigid coaxial cable. The radiating element has a length of 35 mm. The monopole was bent 90°, such that it could be mounted through a hole in the back of the plastic container. The figure also shows the gel present inside the container.

The antennas were mounted in a semicircular array with a 16-cm diameter and an angular spacing of 20° between the individual antennas as shown in Figure 2.6. The measurement system used was the Rohde & Schwarz ZNBT8 16-channel vector network analyzer, this VNA has a dynamic range of up to 140 dB and operates within the frequency range of 9 kHz to 8.5 GHz, even though we only measured within the range of 0.5 GHz to 2.0 GHz with eight

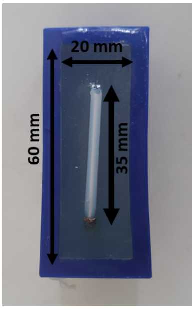

(a)

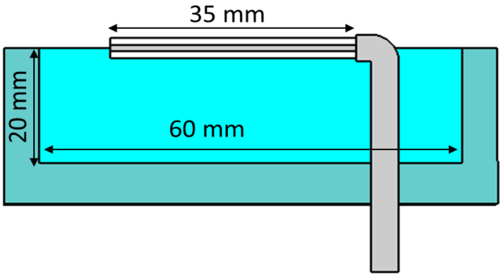

(b)

Figure 2.5: Monopole antenna with cup full of gel: (**a**) top view of antenna; (**b**) side view of antenna taken from paper A.

transmitting/receiving antennas connected via flexible coaxial cables.

Experiments

The experiments were performed using a simplified environment with only two tissues: muscle and blood mimicking phantoms. Muscle mimicking material was used to model the leg of the patient and blood mimicking material as the bleeding accompanying a muscle rupture. Other tissues in the leg such as fat, bone, and skin were omitted for simplicity. The muscle and blood phantoms can be seen in Figure 2.6b. During the measurements, the antennas were applied in direct contact with the surface of the muscle phantom, such that the monopole elements were also in direct contact with the phantom.

To investigate the effects of the different attenuating properties of the gel two different gels were manufactured: a low loss made from regular tap water and 1.5 weight percent (wt%) agar; and a high loss gel made from a mixture of tap water, 1.5 wt% agar and 10 wt% NaCl. The water gel had permittivity $\varepsilon = 79.54$ and conductivity $\sigma = 0.235$ S/m and the lossy gel had permittivity $\varepsilon = 61.37$ and conductivity $\sigma = 11.98$ S/m at 1 GHz. More details about the phantoms and gels are given in paper A.

Figure 2.7 shows a few examples of the measured transmission coefficients (S21 and S41) for the low-loss and high-loss gel. The first notable observation is that the overall amplitude for the high-loss gel was lower than that for the low-loss gel for both S21 and S41. Another observation is that the curve for

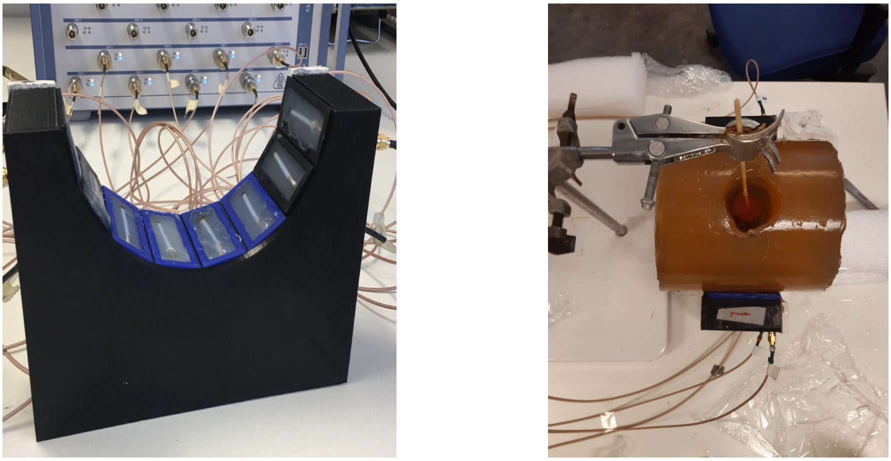

(**a**) (**b**)

Figure 2.6: Measurement setup for probe measurements and image reconstruction: (**a**) semicircular antenna array consisting of 8 antennas; (**b**) muscle phantom in the antenna array, with probes taken from paper A.

the high-loss gel is much smoother than for the low-loss gel. The measured S parameters of the low-loss gel showed a strongly alternating amplitude that appeared to be caused by the multipath waves interfering with the desired object response. In paper A it is shown that the field amplitude inside the muscle phantom was preserved while the surrounding multipath signals were dampened when using the high-loss gel. The lower amplitude seen in this figure for the high-loss gel is a sign that the multipath signals had been removed and the scattering amplitudes from the phantom had been preserved. This is favorable in the subsequent signal processing and image reconstruction.

As shown in Figure 2.7, the low-loss gel had a low conductivity and, therefore a significant level of multipath signals around the system is to be expected. These signals interfere with each other and make the high losses unpredictable as any small change in the experimental setup can create large fluctuations in the measured signals.

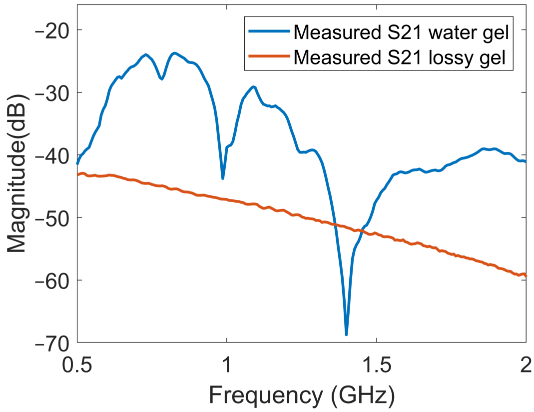

(a)

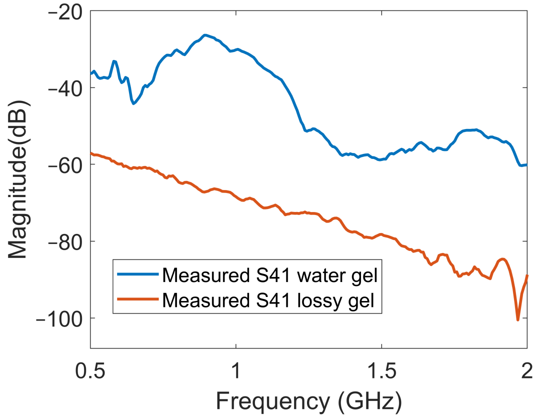

(b)

Figure 2.7: Comparison of transmission coefficients obtained from measured data for low loss and high loss gel : (**a**) results for S21; (**b**) results for S41.

CHAPTER 3

Imaging

Microwave imaging can either show patterns and shapes (qualitative imaging) or imaging of dielectric properties and their spatial distribution (quantitative imaging). Qualitative methods are normally known as radar-based and quantitative methods as tomographic. In this chapter, we will briefly introduce these methods and also discuss the method chosen for our work.

3.1 Tomographic algorithms

Microwave tomographic imaging reconstructs the dielectric properties of the imaging domain using inverse scattering algorithms. These algorithms often involve non-linear and iterative optimization algorithms for image reconstruction and require solving two types of electromagnetic numerical problems: forward and inverse scattering problems. In the forward problem, the electromagnetic propagation in a medium with known dielectric properties and antenna array is calculated; this is a relatively straightforward problem to solve with numerous commercial numerical solvers available. In the inverse problem, the task is to calculate the properties of the dielectric medium based on measured (or simulated) electromagnetic waves that have propagated through the medium between pairs of antennas in the array; this problem is harder to solve since the relationship between the dielectric properties in the imaging domain and the scattered field, in general, is not linear. Several different iterative methods have been developed and used in microwave tomographic applications, like Distorted Born Iterative Method [92], Newton-based methods [93], and Contrast Source Inversion (CSI) [94] can be used.

The iterative inversion methods use simulated electric fields in addition to the measured electric fields. In each iteration, a dielectric distribution is updated incrementally from the previous iteration, and the forward problem is solved. The simulated fields are compared to the measured fields and the dielectric distribution is updated so the difference between the simulated and measured fields is minimized. After multiple iterations, of iteratively refining the dielectric distribution of the corresponding simulated fields, hopefully, converge to a solution that resembles the original dielectric distribution.

The forward problem can be solved using a variety of different methods such as the Finite-Difference Time Domain (FDTD) method [95], [96], the Finite Element method (FEM) [97], [98], Method of Moments (MoM)[99] or the Discrete Dipole Approximation (DDA)[52], [100].

Non-linear reconstruction algorithms require large computational resources and reconstruction times can be very long, up to many hours. This is clearly unfeasible, particularly in clinical settings where an image is often promptly needed. This is true, particularly for three-dimensional (3D) imaging, therefore two dimensional (2D) models and reconstructions are more attractive[52]. Additionally, these inverse problems require regularization due to ill-posedness [101].

3.2 Radar based algorithms

Radar based microwave imaging is another approach used to reconstruct an image. These algorithms exploit time-of-flight measurements of pulses that are transmitted through and scattered by high dielectric contrast objects in the imaging domain[41]. Unlike microwave tomography, where the aim is to reconstruct quantitatively the dielectric parameters within the object, radar based algorithms aim at only reconstructing information on the shape, size, and location of the scatterers[102].

Although providing less detailed information about the object, radar based approaches use less complex algorithms and an image can usually be reconstructed faster compared to a tomographic algorithm.

Radar based approaches use ultra-wideband pulses that are sent into the imaging domain with the purpose of detecting reflected and scattered pulses from strong scatterers [27].

The reconstruction algorithm uses estimated propagation times between antennas and individual pixels in the imaging domain that are correlated with the corresponding measured signals. If a scatterer is present in a particular location the correlation between scattered signals from different directions is high; if a scatterer is not present the correlation is low. An image of the scatterer is created by repeating this process for each pixel in the region of interest. Therefore, the highest intensity point in this intensity map will correspond to the location of the dielectric scatterer [103].

Several imaging algorithms have been reported in the literature examples of such algorithms are the Delay-And-Sum (DAS) beamformer [31], [102], Delay-multiply-And-Sum (DMAS) beamformer [104], Microwave Imaging via Space Time (MIST) [105] and Generalized Likelihood Ratio Test (GLRT) [106], Standard Capon Beamformer(SCB) [107], [108], and Multistatic Adaptive Microwave Imaging (MAMI) beamformer [109].

Despite the fact that these algorithms are much simpler, there are still many challenges involved in this approach. A particular challenge is processing the received signal effectively. The received signals include early-time and late-time content. The early-time content is dominated by reflections from the skin and the late-time content is dominated by the object response. The early-time content needs to be removed from the signal before imaging is done. Otherwise, the desired object response will be drowned in the much larger skin reflection.

3.3 Early-time content removal algorithms

Different methods can be applied to reduce the early-time content. One method includes the use of a priori measurements of a tissue that resembles the object under tests such as lesion-free phantoms, or healthy tissue [104]. An alternative is to use the average of all signals recorded at each channel to estimate the early-time content [31], rotation substraction [78] and the use of different adaptive filtering algorithms [110], [111].

To use the method with a priori data, a reference signal needs to be obtained from measurements of healthy tissue. The reference signal is subtracted from the signal with the object response and since the only change between the healthy and injured signals is the object (in or case blood) then the resulting signal only contains the late time content with the object response. For experimental investigations on phantoms, it is usually possible to perform these before and after measurements. For example, in our experiments, we had a muscle phantom that could be used as healthy tissue (reference) and an injured version (when a blood phantom was inserted) we subtracted the reference signal from the signal coming from the injured version of the phantom to obtain our input to the imaging algorithm. The use of a priori data may not always be possible for clinical applications as it requires measurements of the patient taken before and after injury. In this case, adaptive filtering algorithms may be more suitable.

These algorithms aim to estimate the early-time skin response so it can be removed from the signals before reconstructing the image [42]. Therefore, they are sensitive to measurement variability and noise in the scattering data. Even a small change can create errors or uncertainties in the estimation and removal of the early time signal that could also corrupt the late time object response that one intends to preserve. One important step to help mitigate these problems is to reduce the variability in measurement data and to keep the signals free from undesired scattering that originates from other sources than inside the body.

3.4 Multipath signals deteriorating reconstructed images

As mentioned in 2.3 in paper A, we present an antenna design that makes use of a semisolid gel consisting of a mix of saline, water, and agar. This design helps reduce the variability of the S-parameters by attenuating the signals going outside and around the muscle phantom while still preserving the field amplitude inside the muscle phantom.

In paper A image reconstruction experiments were also realized to show the effectiveness of the antenna using a priori data and the DMAs algorithm. We used phantoms with and without bleeding, subtracted, and, used the differential signals to reconstruct images. The blood phantom had a diameter

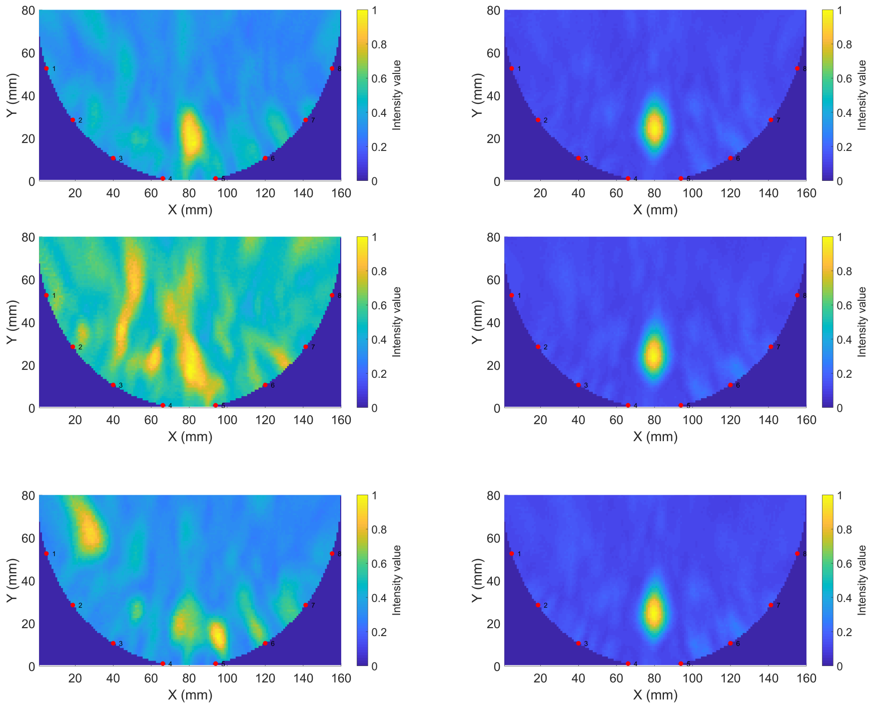

(**a**) Low-loss gel   (**b**) High-loss gel

Figure 3.1: Sample reconstructions using phantom measurements: (**a**) low-loss gel; (**b**) high-loss gel. Taken from paper A.

of 4 cm and when making measurements it was inserted 3 cm above the bottom of the phantom.

Two datasets were used: the low-loss gel and the high-loss gel. For each gel, 15 measurements were taken as a priori measurement (before adding the blood that represents the muscle rupture) and 15 measurements with the blood phantom inserted into the muscle phantom. This means that for each gel, 15 differential signals could be obtained and used as the input signal to the DMAS algorithm. The reason for using multiple measurements (15) was to gather some statistics on the variability in the reconstructed images using the two different gels.

Figure 3.1 shows a few selected reconstructions that were obtained with the measured data for the low-loss gel and the high-loss gel. The reconstructions from the measured data for the low-loss gel showed great variability between images. On the other hand, the reconstructions for the high-loss gel showed fewer artifacts in the background and the blood phantom was always reconstructed in the correct position.

For the case of images reconstructed using the low-loss gels, the reconstruction could be sometimes considered successful like the upper image that looked quite good but with stronger artifacts close to the bottom edge compared to the images obtained using the high-loss gels. Other images looked like the other two images, where some of the artifacts were even larger in amplitude than the reconstructed blood phantom.

Instead of showing all 15 image reconstruction a plot of the reconstructed amplitude were drawn at the vertical line crossing through the center of the muscle phantom. The reconstructed amplitudes are shown in Figure 3.2 and they show the same pattern discussed before.

In paper B the work in paper A was confirmed using blood phantoms with different size and different positions.

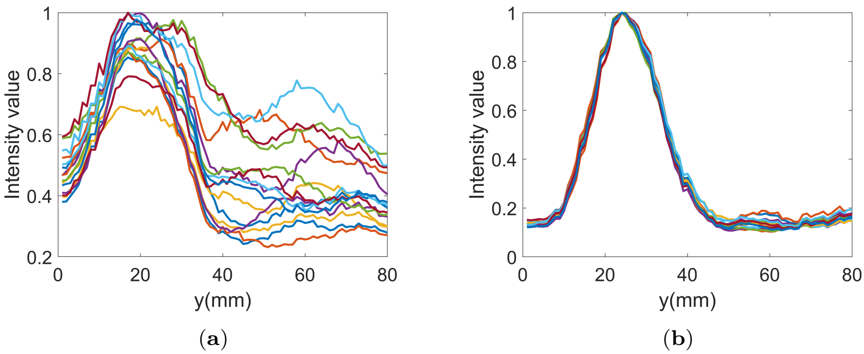

Figure 3.2: Reconstructed data along the line through the center of the imaging domain for 15 images: (**a**) low-loss gel; (**b**) high-loss gel. Taken from paper A.

CHAPTER 4

Summary of included papers

This chapter provides a summary of the included papers.

4.1 Paper A

Laura Guerrero Orozco, Lars Peterson, Andreas Fhager
Microwave Antenna System for Muscle Rupture Imaging with a Lossy Gel to Reduce Multipath Interference
Published in Sensors 2022, 22, 4121
©https://doi.org/10.3390/s22114121 .

The paper presents a novel antenna design and a microwave antenna system for imaging with the purpose of detecting and diagnosing muscle ruptures. A lossy gel was introduced on the back and side of the antennas to attenuate the outgoing and sideways moving waves and contribute to a reduction in undesired multipath signals. Measurements, using tissue-mimicking phantoms, representing muscle and blood, were performed with gels with low loss and gels with high loss. For comparison, corresponding simulations were performed. The results obtained from the simulated and experimental data were in good agreement, they showed that the field amplitudes on the transmission coefficients between antennas decreased with an increased lossiness in the gel while only showing a slight change in the field strength inside the muscle phantom. Additionally, in repeated image reconstruction experiments using the DMAS beamformer algorithm, the high-loss gel antennas showed a more stable and repeatable image reconstruction accuracy in comparison to the low-loss gel. Therefore, we conclude that a reduction in the multipath signals made the signals less corrupted with unpredictable artifacts due to unwanted multipath scattering.

4.2 Paper B

Laura Guerrero Orozco, Lars Peterson, Andreas Fhager
Muscle Rupture Microwave Imaging with a Lossy Gel to Reduce Multipath Interference
Acepted for publication at 17th European Conference on Antenna and Propagation.

This paper present an expansion of the results found in Paper A while using different blood phantom sizes and positions. Measurements were performed using tissue-mimicking phantoms together with both a low-loss gel and a high-loss gel. Two different sizes were used for the blood phantom as well as two different positions inside the muscle phantom. The results confirmed the conclusions found in paper A in different imaging scenarios and showed that reconstructions made with the high-loss gel were more repeatable and stable than the low-loss gel for both sizes and positions.

4.3 Paper C

Xuezhi Zeng, **Laura Guerrero Orozco**
Measurement quality of a software defined radio system for medical diagnostics
Published in the Journal of Engineering-JOE, Volume 2022, Issue 12 December 2022 Pages 1162-1172
©http://dx.doi.org/10.1049/tje2.12196 .

The paper presents a study on the measurement quality of a software-defined radio (SDR) system with the aim to assess if it could be used in microwave applications for medical diagnostics. Sufficient measurement quality is crucial in microwave applications for medical diagnostics and is directly related to diagnostic accuracy. Particularly the high lossy characteristics of biological tissues make the measurements challenging. Therefore, the SDR was tested in order to determine its measurement accuracy and to assess whether it would provide sufficient accuracy to be considered in microwave medical diagnostic systems. In paper C an extensive investigation of the measurement quality of a single SDR board-based system, a two-channel SDR board USRP 2901 from national instruments which is equivalent to the Ettus Research USRP B210 board, was performed. Measurements were performed on an antenna system as well as on a variable attenuator with 70 dB adjustable attenuation range with the purpose of imitating a typical measurement scenario in medical diagnostics. Measurement repeatability, also known as signal-to-noise ratio (SNR), is used to characterize the measurement stability of the system. Previous simulation work showed that an SNR over 15 dB is sufficient for the reconstruction of a specific breast model by using a time-domain tomography approach, and in this work, we showed that this level of accuracy can be achieved with the investigated SDR board. Additionally, we found that the performance of the SDR is superior to a custom-built pulsed time domain system which usually has a maximum SNR of about 40 dB in the investigated frequency range. Furthermore, a calibration strategy is shown in paper C to calibrate the random phase caused by the two different PLLs in the transmitter and the receiver. The calibration strategy made the phase measurements stable. We found there was good measurement repeatability and measurement accuracy of the investigated SDR board benchmarked against a high-performance VNA for a transmission loss up to 70 dB, sufficient for some diagnostics applications.

CHAPTER 5

Concluding Remarks and Future Work

In this thesis, we present the background and results of our work on microwave imaging of muscle rupture detection. The aim of this project is to develop a microwave imaging system that is able to diagnose muscle ruptures. The goal is to develop a system that can complement or in the longer term even replace current imaging modalities, like MRI.

In this thesis, the design and measurement of an antenna with a lossy gel that helps attenuate unwanted multipath signals were presented. This helped attenuate undesired fields outside and around the object under test used in experiments while the results showed that the signal levels inside the object only decreased slightly.

We noted some inconsistencies between the amount of attenuation in the simulated and measured results for the field probe outside of the antenna array. This was possibly due to imperfections in the experiment as well as an overly simplified simulation model. However, the measured trend was clear and in agreement with the simulations, the high-loss gels do attenuate the outgoing signals. Additionally, in image reconstruction experiments using the DMAS algorithm the antennas with the high-loss gel showed more repeatable and stable image reconstruction in comparison to gel with low loss. This indicates that our proposed antenna is feasible in this application.

The measurement quality of a software defined radio (SDR) was explored for biomedical applications. We found that the SDR board has a high enough SNR for microwave tomography.

The next step in this research project is to adapt the antenna array to fit different sizes of legs or phantoms and fine-tune and optimize the antenna characteristics, which may further improve the reduction in unwanted multipath signals and result in enhanced imaging accuracy.

With the phase measurements stabilized, we want to continue exploring the use of the SDR board as a measurement system for the microwave imaging array with the aim to replace the VNA and make the system size smaller and decreasing the cost of the imaging system.

Another future work is the implementation of an early-time content removal algorithm that does not require the a priori measurement of healthy tissue. Future work should also include the use of more realistic phantoms and patients to investigate how image reconstruction is affected by other tissues like bone and fat.

References

[1] F. Arroyo, "Overview of different location of muscle strain," *Muscle Injuries in Sport Medicine*, 2013.

[2] P. Volpi, G. Melegati, D. Tornese, and M. Bandi, "Muscle strains in soccer: A five-year survey of an italian major league team," *Knee Surgery, Sports Traumatology, Arthroscopy*, vol. 12, no. 5, 2004.

[3] C. M. Askling, M. Tengvar, T. Saartok, and A. Thorstensson, "Acute first-time hamstring strains during high-speed running," *The American Journal of Sports Medicine*, vol. 35, no. 2, pp. 197–206, 2007.

[4] K. M. Cross, K. K. Gurka, M. Conaway, and C. D. Ingersoll, "Hamstring strain incidence between genders and sports in ncaa athletics," *Athletic Training amp; Sports Health Care*, vol. 2, no. 3, pp. 124–130, 2010.

[5] C. M. Askling, G. Koulouris, T. Saartok, S. Werner, and T. M. Best, "Total proximal hamstring ruptures: Clinical and mri aspects including guidelines for postoperative rehabilitation," *Knee Surgery, Sports Traumatology, Arthroscopy*, vol. 21, no. 3, pp. 515–533, 2012.

[6] D. A. Connell, M. E. Schneider-Kolsky, J. L. Hoving, *et al.*, "Longitudinal study comparing sonographic and mri assessments of acute and healing hamstring injuries," *American Journal of Roentgenology*, vol. 183, no. 4, pp. 975–984, 2004.

[7] G. Koulouris and D. Connell, "Hamstring muscle complex: An imaging review," *RadioGraphics*, vol. 25, no. 3, pp. 571–586, 2005.

[8] L. Mica, A. Schwaller, C. Stoupis, I. Penka, J. Vomela, and A. Vollenweider, “Avulsion of the hamstring muscle group: A follow-up of 6 adult non-athletes with early operative treatment: A brief report,” *World Journal of Surgery*, vol. 33, no. 8, pp. 1605–1610, 2009.

[9] S. K. Chu and M. E. Rho, “Hamstring injuries in the athlete,” *Current Sports Medicine Reports*, vol. 15, no. 3, pp. 184–190, 2016.

[10] R. Drake, *Gray’s anatomy for students.* Elsevier, 2020.

[11] L. Peterson and P. Renström, *Skador Inom Idrotten: Prevention, behandling och rehabilitering.* Columbus Förlag, 2017.

[12] N. Malliaropoulos, T. Isinkaye, K. Tsitas, and N. Maffulli, “Reinjury after acute posterior thigh muscle injuries in elite track and field athletes,” *The American Journal of Sports Medicine*, vol. 39, no. 2, pp. 304–310, 2010.

[13] C. Woods, “The football association medical research programme: An audit of injuries in professional football–analysis of hamstring injuries,” *British Journal of Sports Medicine*, vol. 38, no. 1, pp. 36–41, 2004.

[14] J. Orchard and H. Seward, “Epidemiology of injuries in the australian football league, seasons 1997–2000,” *British Journal of Sports Medicine*, vol. 36, no. 1, pp. 39–44, 2002.

[15] L. Devlin, “Recurrent posterior thigh symptoms detrimental to performance in rugby union,” *Sports Medicine*, vol. 29, no. 4, pp. 273–287, 2000.

[16] J. Petersen, “Evidence based prevention of hamstring injuries in sport,” *British Journal of Sports Medicine*, vol. 39, no. 6, pp. 319–323, 2005.

[17] J. H. Brooks, C. W. Fuller, S. P. Kemp, and D. B. Reddin, “Incidence, risk, and prevention of hamstring muscle injuries in professional rugby union,” *The American Journal of Sports Medicine*, vol. 34, no. 8, pp. 1297–1306, 2006.

[18] W. E. GARRETT, F. R. RICH, P. K. NIKOLAOU, and J. B. VOGLER, “Computed tomography of hamstring muscle strains,” *Medicine amp; Science in Sports amp; Exercise*, vol. 21, no. 5, 1989.

[19] H.-W. Mueller-Wohlfahrt, L. Haensel, K. Mithoefer, *et al.*, "Terminology and classification of muscle injuries in sport: The munich consensus statement," *British Journal of Sports Medicine*, vol. 47, no. 6, pp. 342–350, 2012.

[20] G. M. Verrall, J. P. Slavotinek, P. G. Barnes, and G. T. Fon, "Diagnostic and prognostic value of clinical findings in 83 athletes with posterior thigh injury," *The American Journal of Sports Medicine*, vol. 31, no. 6, pp. 969–973, 2003.

[21] C. M. Askling, M. Tengvar, T. Saartok, and A. Thorstensson, "Acute first-time hamstring strains during high-speed running," *The American Journal of Sports Medicine*, vol. 35, no. 2, pp. 197–206, 2007.

[22] H. Seward, J. Orchard, H. Hazard, and D. Collinson, "Football injuries in australia at the élite level," *Medical Journal of Australia*, vol. 159, no. 5, pp. 298–301, 1993.

[23] J. Buckley and J. Aler, "Enhancements in the determination of ocean surface wave height from grazing incidence microwave backscatter," in *IGARSS '98. Sensing and Managing the Environment. 1998 IEEE International Geoscience and Remote Sensing. Symposium Proceedings. (Cat. No.98CH36174)*, vol. 5, 1998, 2487–2489 vol.5.

[24] N. K. Nikolova, "Microwave imaging for breast cancer," *IEEE Microwave Magazine*, vol. 12, no. 7, pp. 78–94, 2011.

[25] G. Gennarelli, G. Vivone, P. Braca, F. Soldovieri, and M. G. Amin, "Multiple extended target tracking for through-wall radars," *IEEE Transactions on Geoscience and Remote Sensing*, vol. 53, no. 12, pp. 6482–6494, 2015.

[26] A. Joisel, J. Mallorqui, A. Broquetas, *et al.*, "Microwave imaging techniques for biomedical applications," in *IMTC/99. Proceedings of the 16th IEEE Instrumentation and Measurement Technology Conference (Cat. No.99CH36309)*, vol. 3, 1999, 1591–1596 vol.3.

[27] E. C. Fear, "Microwave imaging of the breast," *Technology in Cancer Research & Treatment*, vol. 4, no. 1, pp. 69–82, 2005.

[28] C. Gabriel, S. Gabriel, and E. Corthout, "The dielectric properties of biological tissues: I. literature survey," *Physics in Medicine and Biology*, vol. 41, no. 11, pp. 2231–2249, 1996.

[29] S. Gabriel, R. W. Lau, and C. Gabriel, "The dielectric properties of biological tissues: III. parametric models for the dielectric spectrum of tissues," *Physics in Medicine and Biology*, vol. 41, no. 11, pp. 2271–2293, 1996.

[30] P. Meaney, M. Fanning, D. Li, S. Poplack, and K. Paulsen, "A clinical prototype for active microwave imaging of the breast," *IEEE Transactions on Microwave Theory and Techniques*, vol. 48, no. 11, pp. 1841–1853, 2000.

[31] X. Li and S. Hagness, "A confocal microwave imaging algorithm for breast cancer detection," *IEEE Microwave and Wireless Components Letters*, vol. 11, no. 3, pp. 130–132, 2001.

[32] E. C. Fear, J. Bourqui, C. Curtis, D. Mew, B. Docktor, and C. Romano, "Microwave breast imaging with a monostatic radar-based system: A study of application to patients," *IEEE Transactions on Microwave Theory and Techniques*, vol. 61, no. 5, pp. 2119–2128, 2013.

[33] S. Y. Semenov and D. R. Corfield, "Microwave tomography for brain imaging: Feasibility assessment for stroke detection," *International Journal of Antennas and Propagation*, vol. 2008, pp. 1–8, 2008.

[34] M. Persson, A. Fhager, H. D. Trefná, *et al.*, "Microwave-based stroke diagnosis making global prehospital thrombolytic treatment possible," *IEEE Transactions on Biomedical Engineering*, vol. 61, no. 11, pp. 2806–2817, 2014.

[35] L. E. Larsen and J. H. Jacobi, "Microwave scattering parameter imagery of an isolated canine kidney," *Medical Physics*, vol. 6, no. 5, pp. 394–403, 1979.

[36] S. Y. Semenov, A. E. Bulyshev, V. G. Posukh, Y. E. Sizov, T. C. Williams, and A. E. Souvorov, "Microwave tomography for detection/imaging of myocardial infarction. i. excised canine hearts," *Annals of Biomedical Engineering*, vol. 31, no. 3, pp. 262–270, 2003.

[37] P. M. Meaney, D. Goodwin, A. H. Golnabi, *et al.*, "Clinical microwave tomographic imaging of the calcaneus: A first-in-human case study of two subjects," *IEEE Transactions on Biomedical Engineering*, vol. 59, no. 12, pp. 3304–3313, 2012.

[38] S. Semenov, J. Kellam, P. Althausen, *et al.*, "Microwave tomography for functional imaging of extremity soft tissues: Feasibility assessment," *Physics in Medicine and Biology*, vol. 52, no. 18, pp. 5705–5719, 2007.

[39] S. Semenov, "Microwave tomography: Review of the progress towards clinical applications," *Philosophical Transactions of the Royal Society A: Mathematical, Physical and Engineering Sciences*, vol. 367, no. 1900, pp. 3021–3042, 2009.

[40] P. Mojabi, M. Ostadrahimi, L. Shafai, and J. LoVetri, "Microwave tomography techniques and algorithms: A review," in *2012 15 International Symposium on Antenna Technology and Applied Electromagnetics*, 2012, pp. 1–4.

[41] M. A. Elahi, B. R. Lavoie, E. Porter, *et al.*, "Comparison of radar-based microwave imaging algorithms applied to experimental breast phantoms," in *2017 XXXIInd General Assembly and Scientific Symposium of the International Union of Radio Science (URSI GASS)*, 2017, pp. 1–4.

[42] M. A. Elahi, "Confocal microwave imaging and artifact removal algorithms for the early detection of breast cancer," Ph.D. dissertation, NUI Galway, 2018.

[43] P. M. Meaney, C. J. Fox, S. D. Geimer, and K. D. Paulsen, "Electrical characterization of glycerin: Water mixtures: Implications for use as a coupling medium in microwave tomography," *IEEE Transactions on Microwave Theory and Techniques*, vol. 65, no. 5, pp. 1471–1478, 2017.

[44] N. Joachimowicz, C. Conessa, T. Henriksson, and B. Duchêne, "Breast phantoms for microwave imaging," *IEEE Antennas and Wireless Propagation Letters*, vol. 13, pp. 1333–1336, 2014.

[45] M. Habibi, D. P. Klemer, and V. Raicu, "Two-dimensional dielectric spectroscopy: Implementation and validation of a scanning open-ended coaxial probe," *Review of Scientific Instruments*, vol. 81, no. 7, p. 075 108, 2010.

[46] J. Garrett and E. Fear, "Stable and flexible materials to mimic the dielectric properties of human soft tissues," *IEEE Antennas and Wireless Propagation Letters*, vol. 13, pp. 599–602, 2014.

[47] P. Meaney, K. Paulsen, S. Geimer, S. Haider, and M. Fanning, "Quantification of 3-d field effects during 2-d microwave imaging," *IEEE Transactions on Biomedical Engineering*, vol. 49, no. 7, pp. 708–720, 2002.

[48] T. Rydholm, A. Fhager, M. Persson, and P. M. Meaney, "A first evaluation of the realistic supelec-breast phantom," *IEEE Journal of Electromagnetics, RF and Microwaves in Medicine and Biology*, vol. 1, no. 2, pp. 59–65, 2017.

[49] Q. Duan, J. H. Duyn, N. Gudino, *et al.*, "Characterization of a dielectric phantom for high-field magnetic resonance imaging applications," *Medical Physics*, vol. 41, no. 10, p. 102 303, 2014.

[50] J. C. Lai, C. B. Soh, E. Gunawan, and K. S. Low, "Uwb microwave imaging for breast cancer detection — experiments with heterogeneous breast phantoms," *Progress In Electromagnetics Research M*, vol. 16, pp. 19–29, 2011.

[51] X. Zeng, A. Fhager, P. Linner, M. Persson, and H. Zirath, "Experimental investigation of the accuracy of an ultrawideband time-domain microwave-tomographic system," *IEEE Transactions on Instrumentation and Measurement*, vol. 60, no. 12, pp. 3939–3949, 2011.

[52] S. Hosseinzadegan, A. Fhager, M. Persson, S. D. Geimer, and P. M. Meaney, "Discrete dipole approximation-based microwave tomography for fast breast cancer imaging," *IEEE Transactions on Microwave Theory and Techniques*, vol. 69, no. 5, pp. 2741–2752, 2021.

[53] A. Fhager, P. Hashemzadeh, and M. Persson, "Reconstruction quality and spectral content of an electromagnetic time-domain inversion algorithm," *IEEE Transactions on Biomedical Engineering*, vol. 53, no. 8, pp. 1594–1604, 2006.

[54] M. Klemm, I. J. Craddock, J. A. Leendertz, A. Preece, and R. Benjamin, "Radar-based breast cancer detection using a hemispherical antenna array—experimental results," *IEEE Transactions on Antennas and Propagation*, vol. 57, no. 6, pp. 1692–1704, 2009.

[55] M. Bassi, M. Caruso, M. S. Khan, A. Bevilacqua, A.-D. Capobianco, and A. Neviani, "An integrated microwave imaging radar with planar antennas for breast cancer detection," *IEEE Transactions on Microwave Theory and Techniques*, vol. 61, no. 5, pp. 2108–2118, 2013.

[56] X. Zeng, A. Fhager, Z. He, M. Persson, P. Linner, and H. Zirath, "Development of a time domain microwave system for medical diagnostics," *IEEE Transactions on Instrumentation and Measurement*, vol. 63, no. 12, pp. 2931–2939, 2014.

[57] L. Kranold, M. Taherzadeh, F. Nabki, M. Coates, and M. Popović, "Microwave breast screening prototype: System miniaturization with ic pulse radio," *IEEE Journal of Electromagnetics, RF and Microwaves in Medicine and Biology*, vol. 5, no. 2, pp. 168–178, 2021.

[58] A. T. Mobashsher, A. M. Abbosh, and Y. Wang, "Microwave system to detect traumatic brain injuries using compact unidirectional antenna and wideband transceiver with verification on realistic head phantom," *IEEE Transactions on Microwave Theory and Techniques*, vol. 62, no. 9, pp. 1826–1836, 2014.

[59] A. Santorelli, M. Chudzik, E. Kirshin, *et al.*, "Experimental demonstration of pulse shaping for time-domain microwave breast imaging," *Progress In Electromagnetics Research*, vol. 133, pp. 309–329, 2013.

[60] X. Zeng, A. Fhager, M. Persson, and H. Zirath, "Performance evaluation of a time-domain microwave system for medical diagnostics," *IEEE Transactions on Instrumentation and Measurement*, vol. 68, no. 8, pp. 2880–2889, 2019.

[61] M. Hines and H. Stinehelfer, "Time-domain oscillographic microwave network analysis using frequency-domain data," *IEEE Transactions on Microwave Theory and Techniques*, vol. 22, no. 3, pp. 276–282, 1974.

[62] Z. Maricevic, T. Sarkar, Y. Hua, and A. Djordjevic, "Time-domain measurements with the hewlett-packard network analyzer hp 8510 using the matrix pencil method," *IEEE Transactions on Microwave Theory and Techniques*, vol. 39, no. 3, pp. 538–547, 1991.

[63] E. Fear, J. Sill, and M. Stuchly, "Experimental feasibility study of confocal microwave imaging for breast tumor detection," *IEEE Transactions on Microwave Theory and Techniques*, vol. 51, no. 3, pp. 887–892, 2003.

[64] J. Sill and E. Fear, "Tissue sensing adaptive radar for breast cancer detection—experimental investigation of simple tumor models," *IEEE Transactions on Microwave Theory and Techniques*, vol. 53, no. 11, pp. 3312–3319, 2005.

[65] D. Cook, H. Brown, I. Widanapathirana, *et al.*, "Case report: Preliminary images from an electromagnetic portable brain scanner for diagnosis and monitoring of acute stroke," *Frontiers in Neurology*, vol. 12, 2021.

[66] T. Ulversoy, "Software defined radio: Challenges and opportunities," *IEEE Communications Surveys & Tutorials*, vol. 12, no. 4, pp. 531–550, 2010.

[67] M. Sadiku and C. Akujuobi, "Software-defined radio: A brief overview," *IEEE Potentials*, vol. 23, no. 4, pp. 14–15, 2004.

[68] *Usrp-2901*.

[69] J. Marimuthu, K. S. Bialkowski, and A. M. Abbosh, "Software-defined radar for medical imaging," *IEEE Transactions on Microwave Theory and Techniques*, vol. 64, no. 2, pp. 643–652, 2016.

[70] A. E. Stancombe, K. S. Bialkowski, and A. M. Abbosh, "Portable microwave head imaging system using software-defined radio and switching network," *IEEE Journal of Electromagnetics, RF and Microwaves in Medicine and Biology*, vol. 3, no. 4, pp. 284–291, 2019.

[71] P. Meaney, A. Hartov, T. Raynolds, *et al.*, "Low cost, high performance, 16-channel microwave measurement system for tomographic applications," *Sensors*, vol. 20, no. 18, 2020, ISSN: 1424-8220.

[72] M. Persson, A. Fhager, H. D. Trefná, *et al.*, "Microwave-based stroke diagnosis making global prehospital thrombolytic treatment possible," *IEEE Transactions on Biomedical Engineering*, vol. 61, no. 11, pp. 2806–2817, 2014.

[73] X. Li, M. Jalilvand, Y. L. Sit, and T. Zwick, "A compact double-layer on-body matched bowtie antenna for medical diagnosis," *IEEE Transactions on Antennas and Propagation*, vol. 62, no. 4, pp. 1808–1816, 2014.

[74] H. Bahramiabarghouei, E. Porter, A. Santorelli, B. Gosselin, M. Popović, and L. A. Rusch, "Flexible 16 antenna array for microwave breast cancer detection," *IEEE Transactions on Biomedical Engineering*, vol. 62, no. 10, pp. 2516–2525, 2015.

[75] M. Tommer, K. G. Kjelgård, and T. S. Lande, "Body coupled wideband monopole antenna," in *2016 Loughborough Antennas Propagation Conference (LAPC)*, 2016, pp. 1–5.

[76] A. M. de Oliveira, A. M. de Oliveira Neto, M. B. Perotoni, *et al.*, "A fern antipodal vivaldi antenna for near-field microwave imaging medical applications," *IEEE Transactions on Antennas and Propagation*, vol. 69, no. 12, pp. 8816–8829, 2021.

[77] X. Li, L. Zwirello, M. Jalilvand, and T. Zwick, "Design and near-field characterization of a planar on-body uwb slot-antenna for stroke detection," in *2012 IEEE International Workshop on Antenna Technology (iWAT)*, 2012, pp. 201–204.

[78] M. Klemm, I. J. Craddock, A. Preece, J. Leendertz, and R. Benjamin, "Evaluation of a hemi-spherical wideband antenna array for breast cancer imaging," *Radio Science*, vol. 43, no. 06, pp. 1–15, 2008.

[79] S.-H. Son, "Preclinical prototype development of a microwave tomography system for breast cancer detection," *ETRI Journal*, vol. 32, no. 6, pp. 901–910, 2010.

[80] P. M. Meaney, F. Shubitidze, M. W. Fanning, M. Kmiec, N. R. Epstein, and K. D. Paulsen, "Surface wave multipath signals in near-field microwave imaging," *International Journal of Biomedical Imaging*, vol. 2012, pp. 1–11, 2012.

[81] A. Fhager, S. K. Padhi, M. Persson, and J. Howard, "Antenna modeling and reconstruction accuracy of time domain-based image reconstruction in microwave tomography," *International Journal of Biomedical Imaging*, vol. 2013, pp. 1–14, 2013.

[82] L. E. Larsen and J. H. Jacobi, "Microwave interrogation of dielectric targets. part i: By scattering parameters," *Medical Physics*, vol. 5, no. 6, pp. 500–508, 1978.

[83] J. H. Jacobi and L. E. Larsen, "Microwave interrogation of dielectric targets. part ii: By microwave time delay spectroscopy," *Medical Physics*, vol. 5, no. 6, pp. 509–513, 1978.

[84] Y. Fang, K. Bakian-Dogaheh, J. Stang, A. Tabatabaeenejad, and M. Moghaddam, “A versatile and shelf-stable dielectric coupling medium for microwave imaging,” *IEEE Transactions on Biomedical Engineering*, vol. 69, no. 8, pp. 2701–2712, 2022.

[85] P. M. Meaney, “Addressing multipath signal corruption in microwave tomography and the influence on system design and algorithm development,” *Open Access Journal of Biomedical Engineering and Biosciences*, vol. 1, no. 1, 2018.

[86] P. M. Meaney, C. J. Fox, S. D. Geimer, and K. D. Paulsen, “Electrical characterization of glycerin: Water mixtures: Implications for use as a coupling medium in microwave tomography,” *IEEE Transactions on Microwave Theory and Techniques*, vol. 65, no. 5, pp. 1471–1478, 2017.

[87] J. Chang, K. Paulsen, P. Meaney, and M. Fanning, “Non-invasive thermal assessment of tissue phantoms using an active near field microwave imaging technique,” English (US), *International Journal of Hyperthermia*, vol. 14, no. 6, pp. 513–534, 1998, ISSN: 0265-6736.

[88] J. Bourqui, J. Garrett, and E. Fear, “Measurement and analysis of microwave frequency signals transmitted through the breast,” *International Journal of Biomedical Imaging*, vol. 2012, pp. 1–11, 2012.

[89] C. J. Fox, P. M. Meaney, F. Shubitidze, L. Potwin, and K. D. Paulsen, “Characterization of an implicitly resistively-loaded monopole antenna in lossy liquid media,” *International Journal of Antennas and Propagation*, vol. 2008, pp. 1–9, 2008.

[90] P. Meaney, K. Paulsen, and J. Chang, “Near-field microwave imaging of biologically-based materials using a monopole transceiver system,” *IEEE Transactions on Microwave Theory and Techniques*, vol. 46, no. 1, pp. 31–45, 1998.

[91] C. Gilmore, A. Zakaria, S. Pistorius, and J. LoVetri, “Microwave imaging of human forearms: Pilot study and image enhancement,” *International Journal of Biomedical Imaging*, vol. 2013, pp. 1–17, 2013.

[92] F. Gao, B. D. Van Veen, and S. C. Hagness, “Sensitivity of the distorted born iterative method to the initial guess in microwave breast imaging,” *IEEE Transactions on Antennas and Propagation*, vol. 63, no. 8, pp. 3540–3547, 2015.

[93] T. Takenaka, H. Jia, and T. Tanaka, "Microwave imaging of electrical property distributions by a forward-backward time-stepping method," *Journal of Electromagnetic Waves and Applications*, vol. 14, no. 12, pp. 1609–1626, 2000.

[94] A. Zakaria, C. Gilmore, and J. LoVetri, "Finite-element contrast source inversion method for microwave imaging," *Inverse Problems*, vol. 26, no. 11, p. 115 010, 2010.

[95] A. Fhager, S. K. Padhi, and J. Howard, "3d image reconstruction in microwave tomography using an efficient fdtd model," *IEEE Antennas and Wireless Propagation Letters*, vol. 8, pp. 1353–1356, 2009.

[96] A. Taflove and S. C. Hagness, *Computational electrodynamics: The finite-difference time-domain method.* Artech House, 2010.

[97] K. Paulsen, P. Meaney, M. Moskowitz, and J. Sullivan, "A dual mesh scheme for finite element based reconstruction algorithms," *IEEE Transactions on Medical Imaging*, vol. 14, no. 3, pp. 504–514, 1995.

[98] A. M. Abbosh, B. Mohammed, and K. S. Bialkowski, "Differential microwave imaging of the breast pair," *IEEE Antennas and Wireless Propagation Letters*, vol. 15, pp. 1434–1437, 2016.

[99] A. Franchois and C. Pichot, "Microwave imaging-complex permittivity reconstruction with a levenberg-marquardt method," *IEEE Transactions on Antennas and Propagation*, vol. 45, no. 2, pp. 203–215, 1997.

[100] T. M. Grzegorczyk, P. M. Meaney, P. A. Kaufman, R. M. diFlorio-Alexander, and K. D. Paulsen, "Fast 3-d tomographic microwave imaging for breast cancer detection," *IEEE Transactions on Medical Imaging*, vol. 31, no. 8, pp. 1584–1592, 2012.

[101] A. N. Tikhonov, *Numerical methods for the solution of ill-posed problems.* Springer, 2011.

[102] S. Hagness, A. Taflove, and J. Bridges, "Two-dimensional fdtd analysis of a pulsed microwave confocal system for breast cancer detection: Fixed-focus and antenna-array sensors," *IEEE Transactions on Biomedical Engineering*, vol. 45, no. 12, pp. 1470–1479, 1998.

[103] S. Semenov, A. Bulyshev, A. Abubakar, *et al.*, “Microwave-tomographic imaging of the high dielectric-contrast objects using different image-reconstruction approaches,” *IEEE Transactions on Microwave Theory and Techniques*, vol. 53, no. 7, pp. 2284–2294, 2005.

[104] H. Been Lim, N. Thi Tuyet Nhung, E.-P. Li, and N. Duc Thang, “Confocal microwave imaging for breast cancer detection: Delay-multiply-and-sum image reconstruction algorithm,” *IEEE Transactions on Biomedical Engineering*, vol. 55, no. 6, pp. 1697–1704, 2008.

[105] E. Bond, X. Li, S. Hagness, and B. Van Veen, “Microwave imaging via space-time beamforming for early detection of breast cancer,” *IEEE Transactions on Antennas and Propagation*, vol. 51, no. 8, pp. 1690–1705, 2003.

[106] S. Davis, H. Tandradinata, S. Hagness, and B. Van Veen, “Ultrawideband microwave breast cancer detection: A detection-theoretic approach using the generalized likelihood ratio test,” *IEEE Transactions on Biomedical Engineering*, vol. 52, no. 7, pp. 1237–1250, 2005.

[107] P. Stoica, Z. Wang, and J. Li, “Robust capon beamforming,” *IEEE Signal Processing Letters*, vol. 10, no. 6, pp. 172–175, 2003.

[108] J. Li, P. Stoica, and Z. Wang, “On robust capon beamforming and diagonal loading,” *IEEE Transactions on Signal Processing*, vol. 51, no. 7, pp. 1702–1715, 2003.

[109] Y. Xie, B. Guo, L. Xu, J. Li, and P. Stoica, “Multistatic adaptive microwave imaging for early breast cancer detection,” *IEEE Transactions on Biomedical Engineering*, vol. 53, no. 8, pp. 1647–1657, 2006.

[110] B. Maklad, C. Curtis, E. C. Fear, and G. G. Messier, “Neighborhood-based algorithm to facilitate the reduction of skin reflections in radar-based microwave imaging,” *Progress In Electromagnetics Research B*, vol. 39, pp. 115–139, 2012.

[111] M. A. Elahi, M. Glavin, E. Jones, and M. O’Halloran, “Artifact removal algorithms for microwave imaging of the breast,” *Progress In Electromagnetics Research*, vol. 141, pp. 185–200, 2013.